

Article

Effect of High-Temperature Heat Treatment on Strengthening Mechanism of AlCoCrFeNi Component Fabricated by LMD

Zheng Pang¹, Jin Yang¹, Sunusi Marwana Manladan², Yangchuan Cai^{3,*}  and Jian Han³

¹ Jiangsu Baosteel Fine Wire & Cord Co., Ltd., Nantong 226114, China; 170408@baosteel.com (Z.P.); yangjin579123@baosteel.com (J.Y.)

² School of Materials Science and Engineering, Tianjin University, Tianjin 300072, China; smmanladan@tju.edu.cn

³ School of Materials Science and Engineering, Tianjin University of Technology, Tianjin 300384, China; hj_tjut@vip.126.com

* Correspondence: 18622265848@163.com; Tel.: +86-18622265848

Abstract: In the present study; an AlCoCrFeNi high-entropy alloy (HEA) component was produced by laser melting deposition (LMD) technique. Then; a heat-treatment process based on the detection results of Differential Scanning Calorimeter (DSC) was used. The effects of heat treatment on the phase transition; microstructure and mechanical properties of the AlCoCrFeNi component were systematically studied. The results showed that low-temperature heat treatment (600 °C) had little effect on the microstructure and mechanical properties of component. The 800 °C heat treatment precipitated σ and face-center cubic (FCC) phases near grain boundaries in the component. The high dislocation capacity of FCC phase and precipitation strengthening of σ phase improved the strength and plasticity of this component. However; hard and brittle σ phase was not conducive to uniform distribution of microhardness. High-temperature heat treatment (1000 °C) caused the σ phase to remelt and increased FCC phase content at grain boundaries; resulting in a significant increase in strength and plasticity. Although the microhardness of the AlCoCrFeNi component after this heat treatment was reduced; the good strength and plasticity will facilitate its application in the structural field.

Keywords: AlCoCrFeNi-HEA component; heat treatment; microstructure; mechanical properties; σ phase



Citation: Pang, Z.; Yang, J.; Manladan, S.M.; Cai, Y.; Han, J. Effect of High-Temperature Heat Treatment on Strengthening Mechanism of AlCoCrFeNi Component Fabricated by LMD. *Metals* **2022**, *12*, 767. <https://doi.org/10.3390/met12050767>

Academic Editors: Jingwei Zhao, Zhengyi Jiang, Leszek Adam Dobrzański and Chong Soo Lee

Received: 6 April 2022
Accepted: 21 April 2022
Published: 29 April 2022

Publisher's Note: MDPI stays neutral with regard to jurisdictional claims in published maps and institutional affiliations.



Copyright: © 2022 by the authors. Licensee MDPI, Basel, Switzerland. This article is an open access article distributed under the terms and conditions of the Creative Commons Attribution (CC BY) license (<https://creativecommons.org/licenses/by/4.0/>).

1. Introduction

AlCoCrFeNi was one of the first investigated high-entropy alloys (HEAs) [1]. Good mechanical properties [2–5] have led to significant attention for this HEA. The advantages of AlCoCrFeNi-HEA encouraged the use of a variety of preparation methods. However, in practical application, AlCoCrFeNi components are non-equilibrium solidification-state-prepared by casting or additive manufacturing. Therefore, in order to make the structure and performance of the AlCoCrFeNi components stable, heat treatment, which can effectively reduce the residual stress and supersaturated solid solution generated in the non-equilibrium preparation process, is essential.

A. Munitz et al. [6] prepared AlCoCrFeNi-HEA by arc melting. Heat treatment between 650 °C and 975 °C led to the transformation of body-center cubic (BCC) matrix into σ phase in the interdendritic region, and heat treatment at 1100 °C led to the transformation of σ phase into BCC structure. J.T. Liang et al. [7] fabricated AlCoCrFeNi-HEA powder by gas atomization process. After annealing at 900 °C for 3 h, the phase composition consisted of face-center cubic (FCC) + BCC phase, and after 12 h, the phase composition consists of FCC, BCC and σ phase. P.F. Zhou et al. [8] prepared AlCoCrFeNi-HEA using spark plasma compaction (SPS), nano σ phase was formed during annealing. With the increase of annealing temperature, the size and quantity of nanoscale precipitation increased. D.Y. Lin et al. [9]

only obtained AlNi_3 phase by vacuum heat treatment of the AlCoCrFeNi-HEA coating prepared by supersonic air-plasma spraying. L.Q. Wang et al. [10] prepared thick-layer AlCoCrFeNi-HEA coating by means of atmosphere plasma spraying (APS). With the increase of temperature in the range of 600–900 °C, rod-shaped FCC structure was embedded into the BCC matrix, and grew together as the temperature rose. W.M. Guo et al. [11] found that the laser-cladding layer of AlCoCrFeNi-HEA can obtain BCC single phase after 700 °C treatment. Large number of FCC and σ particles distributed on the grain boundaries of BCC phase matrix after 900 °C and 1100 °C heat treatment.

For AlCoCrFeNi-HEA obtained by different preparation methods, there were obvious differences in the heat-treatment process and corresponding microstructure evolution. The existence of such differences urges scholars to establish the coupling relationship between the preparation method of AlCoCrFeNi-HEA and the heat-treatment process, in order to obtain corresponding excellent properties and promote the future development and industrial application of this HEA [12–14]. In recent years, additive manufacturing (AM) has gained increasing attention in the field of HEAs manufacturing, as it not only can effectively overcome the problems in traditional preparation methods such as element segregation, shrinkage and coarse grains, but also fabricate the complex structure [15–17].

L.F. Huang et al. [18] successfully synthesized AlCoCrFeNi-HEA with BCC structure by laser-melting deposition (LMD). Q.X. Sui et al. [19] prepared AlCoCrFeNi-HEA with BCC structure using the direct-energy deposition (DED) method, and the microstructure changed from a columnar grain structure to an equiaxed dendrite structure. P.D. Niu et al. [20] fabricated AlCoCrFeNi-HEA by selective laser melting (SLM), and the SLM sample was composed of disordered BCC and ordered BCC (B2). AlCoCrFeNi-HEA obtained by different kinds of additive manufacturing methods had a basically similar microstructure. However, a small number of scholars found differences in the evolution of their microstructures after heat treatment with different additive components. R. Wang et al. [21] used direct laser fabrication (DLF) to prepare AlCoCrFeNi-HEA . After aging at 800 °C, 1000 °C and 1200 °C, needlelike and platelike FCC phases precipitated along grain boundaries. H.R. Sistla et al. [22] successfully fabricated AlFeCoCrNi-HEA with laser-aided direct-metal deposition, and annealing at high temperature led to the σ phase transition. Therefore, different additive manufacturing methods should be matched with the corresponding heat treatment process to obtain AlFeCoCrNi components with better mechanical properties than those before heat treatment.

Consequently, in the present study, AlCoCrFeNi-HEA components were fabricated by LMD. The influence of high-temperature conditions on the evolution of phases, microstructure, and properties of the components were investigated systematically.

2. Experimental Procedures

2.1. Raw Materials and Fabrication of the AlCoCrFeNi Components

The base metal used in the LMD process was 45# steel (Huijiaying machinery processing factory, Tianjin, China), and its chemical composition is shown Table 1. The surface of the 45# steel was cleaned with acetone before the LMD process. The AlCoCrFeNi HEA powders used in this study were purchased from Jiangsu Vilory Advanced Materials Technology Co., Ltd. (Jiangsu, China). The LMD process was performed using a HANSGS-RJ0016-F3K laser machine (Han's Laser Technology Industry Group Co., Ltd., Shenzhen, China), as shown in Figure 1a. The LMD parameters were as follows: Laser power of 1300 W, scanning velocity of 6 mm/s, laser beam spot diameter (negative defocus) of 3 mm, argon shielding gas at flow rate of 25 mL/min, transfer speed of 2.5 rpm, multi-track overlap ratio of 30%, and lift distance of 1 mm in Z direction.

Table 1. Chemical composition of 45# steel (wt.%).

C	Mn	P	S	Si	Cr	Ni	Cu	Fe
0.046	0.065	0.035	0.035	0.24	0.025	0.025	0.25	Bal.

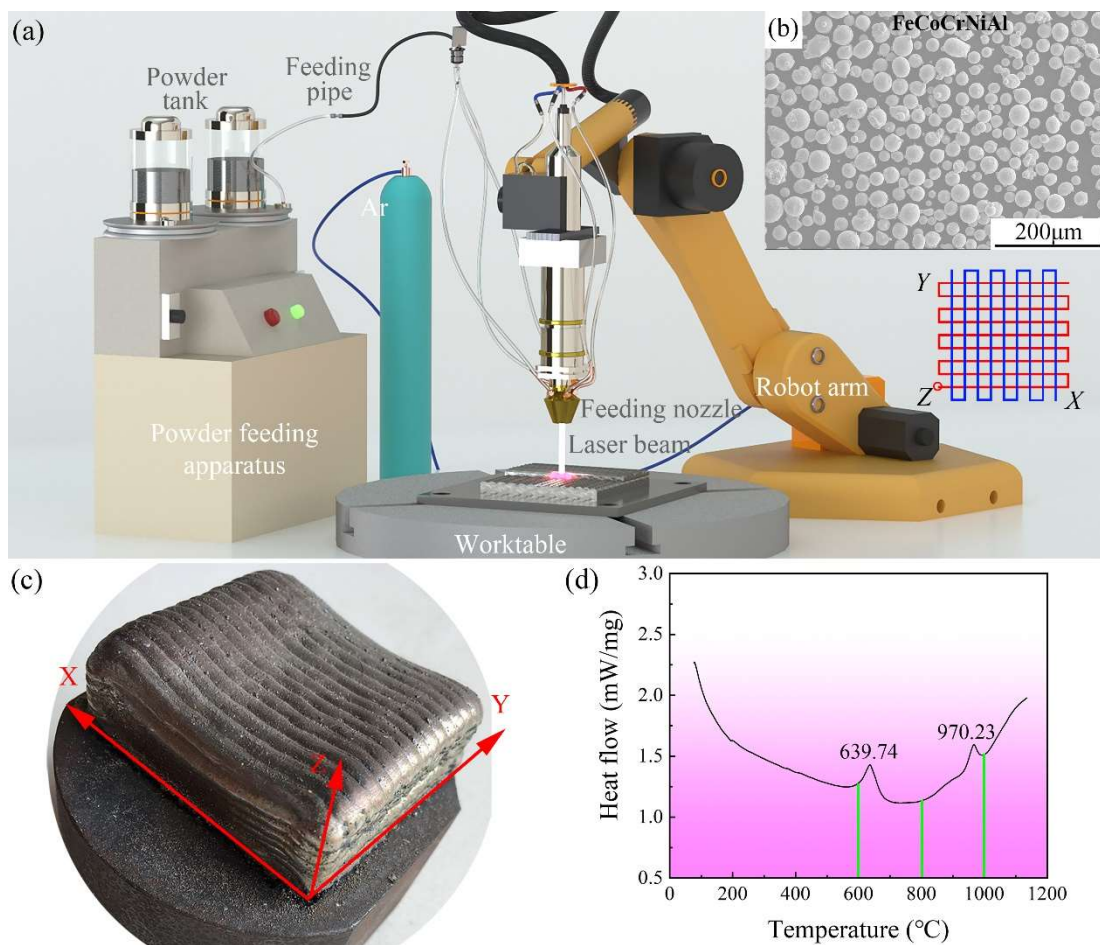


Figure 1. (a) Laser-melting deposition system; (b) AlCoCrFeNi powders; (c) the fabricated AlCoCrFeNi component; (d) DSC analysis results for the fabricated AlCoCrFeNi component.

The molar ratio of the alloying elements in the AlCoCrFeNi HEA powders was 1:1:1:1:1 (Al:Co:Cr:Fe:Ni). The purity of the HEA powder was 99.0–99.5% and its granularity was 50–150 μm , as shown in Figure 1b. The particles mainly have a low diameter ($\sim 70 \mu\text{m}$). The AlCoCrFeNi components were produced using a vertical ‘S’ type trajectory in plane (X–Y). The Z direction is the building direction. To prevent the formation of cold cracks, the bottom of base metal was heated to a temperature of 500 $^{\circ}\text{C}$. The fabricated AlCoCrFeNi component is shown in Figure 1c.

2.2. High-Temperature Heat Treatment

The phase-transition temperature for the AlCoCrFeNi component was accurately measured by a TGA/DSC 1/1600 Differential Scanning Calorimeter (DSC, Mettler Toledo Technology (China) Co., Ltd., Shanghai, China) with a heating rate of 45 $^{\circ}\text{C}/\text{min}$. As shown in the results (Figure 1d), two transition temperatures were obtained (639.74 $^{\circ}\text{C}$ and 970.23 $^{\circ}\text{C}$). Therefore, in the present work, temperatures of 600 $^{\circ}\text{C}$, 800 $^{\circ}\text{C}$ and 1000 $^{\circ}\text{C}$ were selected for the heat-treatment process. The heat treatment is carried out on the furnace of model TL1700 (Tianjin Marvel Technology Co., Ltd., Tianjin, China) and the annealing atmosphere is vacuum. The heat treatment process involved the following steps: heating from room temperature to 200 $^{\circ}\text{C}$ for 60 min and then heating from 200 $^{\circ}\text{C}$ to the heat treatment temperature (600 $^{\circ}\text{C}$, 800 $^{\circ}\text{C}$ or 1000 $^{\circ}\text{C}$) at a rate of 5 $^{\circ}\text{C}/\text{min}$. After reaching the required temperature for 5 h, it shall be cooled in the furnace.

2.3. Microstructure Characterization

Metallographic samples were cut from the fabricated AlCoCrFeNi components, ground and polished as per standard metallographic procedure. The identification of phases in the component was conducted using a D8 advanced X-ray diffractometer (Rigaku D/max/2500PC, Hitachi Co., Ltd., Tokyo, Japan) at a scanning speed of $4^\circ \cdot \text{min}^{-1}$ and a range of 20° to 100° . The XRD data obtained was analyzed using Origin Pro 8.5 software. Electron backscattered diffraction (EBSD) analysis was conducted using a TESCAN MAIA3 machine (Tisken (China) Co., Ltd., Brno, Czech) equipped with Channel 5 software. Step sizes of $2 \mu\text{m}$ and $4 \mu\text{m}$ were used. Furthermore, transmission electron microscope (TEM, FEI Co., Ltd., Hillsboro, OR, USA) was used to obtain high magnification electron images and to determine the distribution of alloying elements and selected area diffraction patterns.

2.4. Mechanical Properties

Compression test was conducted using a CSS-44100 electronic universal testing machine at a loading rate of 1 mm/min . Three compression-test samples were produced for each condition of the AlCoCrFeNi component, with a diameter of 4 mm and length of 6 mm . The rotation symmetry axes of the cylindrical samples were perpendicular to the plane (X-Y). Quanta FEG 250 scanning electron microscope (SEM Hitachi Co., Ltd., Tokyo, Japan) was used to characterize the fracture surface after the compression test.

The micro-hardness of the AlCoCrFeNi components was measured using MHV2000 micro-hardness tester, under a load of 500 g and 15 s dwell time. The test was conducted on the X-Z plane, and 10 points were tested in both the X and Z directions, making a total of 100 points. The tests were conducted at intervals of 0.2 mm .

3. Results and Discussion

3.1. Phase and Microstructure of the AlCoCrFeNi Components

The XRD patterns of the AlCoCrFeNi components before and after the heat treatment processes are presented in Figure 2. At present, there is no PDF card of high-entropy alloy, so it is calibrated with reference to the diffraction patterns of FCC and BCC structural materials. The as-fabricated AlCoCrFeNi component consisted mainly of BCC phase. No phase transformations occurred after the heat treatment at 600°C . After the heat treatment at 800°C , both FCC and σ phases appeared. However, after the heat treatment at 1000°C , the σ phase disappeared and the FCC and BCC phases remained. The phase transformations observed in the AlCoCrFeNi components after the heat-treatment processes in this study are consistent with the results of the previous studies [22–26].

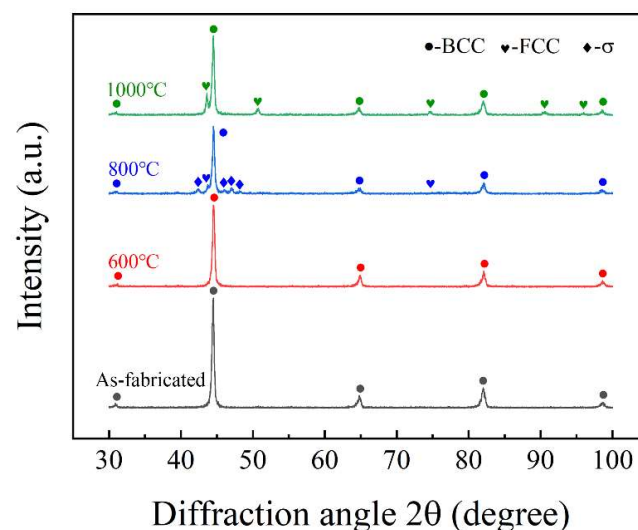


Figure 2. XRD results of the AlCoCrFeNi components before and after high-temperature treatment.

The results of the XRD analysis in Figure 2 shows the types of phases in the Al-CoCrFeNi components before and after high-temperature treatment. However, the phase distribution could not be determined using XRD. Therefore, high-power EBSD was used to determine the phase in the components, as shown in Figure 3. Compared with the as-fabricated component, the phase in the component heat-treated at 600 °C did not change, as shown in Figure 3a,b, which is consistent with the XRD results. As shown in Figure 3c, FCC phase precipitated at the grain boundaries of the BCC phase in the component heat-treated at 800 °C, but σ phase was not detected. The contents of FCC and BCC phases in this component were 1.62% and 98.4%, respectively. Since the XRD and EBSD analysis gave contradictory σ phase results, the type and distribution of phase structures in the 800 °C heat-treated component were further analyzed by TEM. The FCC and BCC phases in the component are rich in Al-Ni and Cr-Fe-Co, respectively, while the σ phase is an hexagonal close-packed (HCP) structure rich in Cr-Fe-Co, as shown in Figure 4b,c. Both the FCC and σ phases are mainly distributed near the grain boundaries (GB), and the FCC phase is mainly elongated, while the σ phase tends to be elliptical, as shown in Figure 4a. Phase boundary (PB), GB, HCP, FCC and BCC are shown in Figure 4.

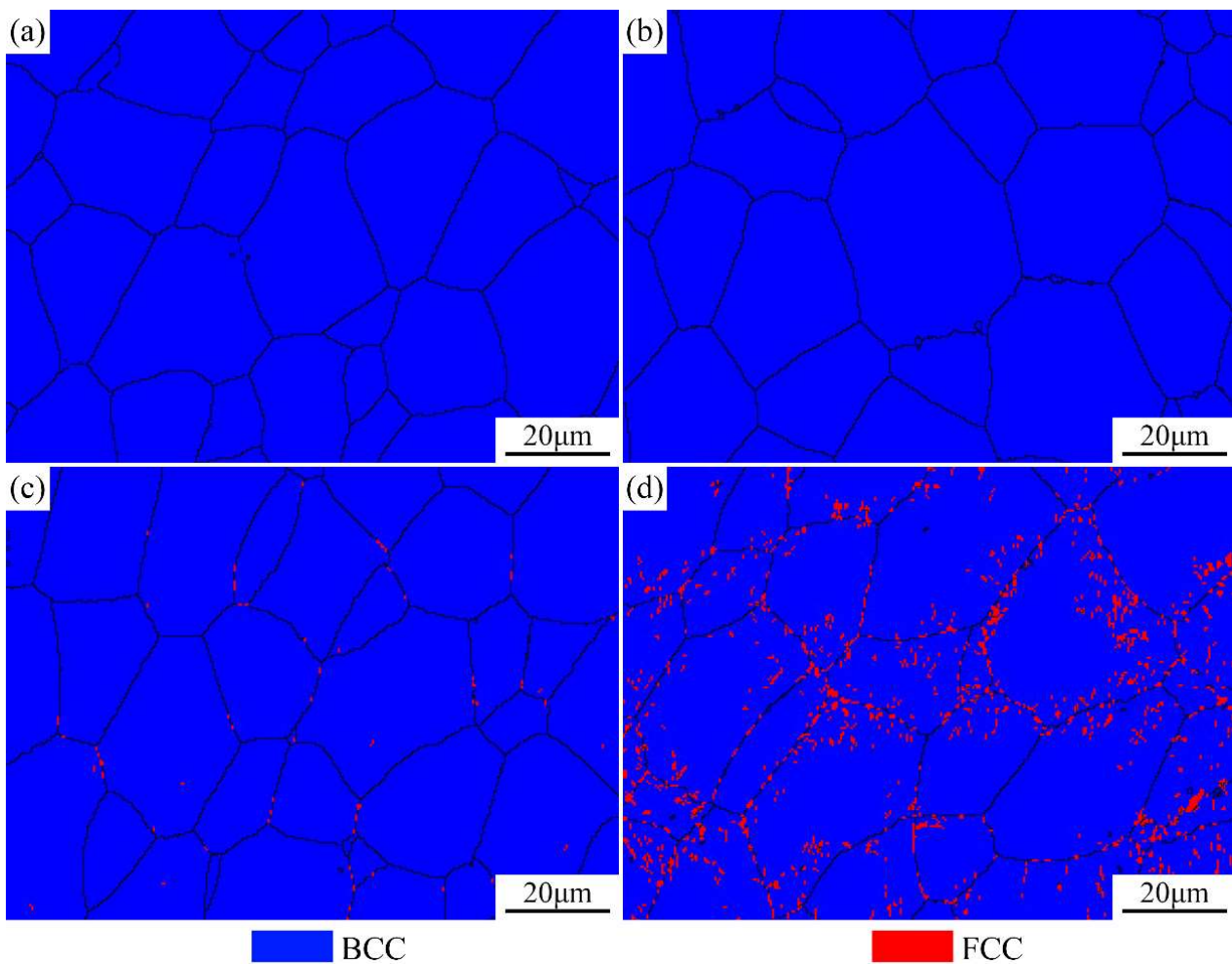


Figure 3. EBSD-phase analysis results of the AlCoCrFeNi components before and after high-temperature treatment: (a) as-fabricated; heat-treated at (b) 600 °C, (c) 800 °C, and (d) 1000 °C.

The content of the FCC phase in the component heat-treated at 1000 °C increased significantly to about 12.7%, as shown in Figure 3d. In addition to being distributed at the grain boundaries, the FCC phase also precipitated inside the grains.

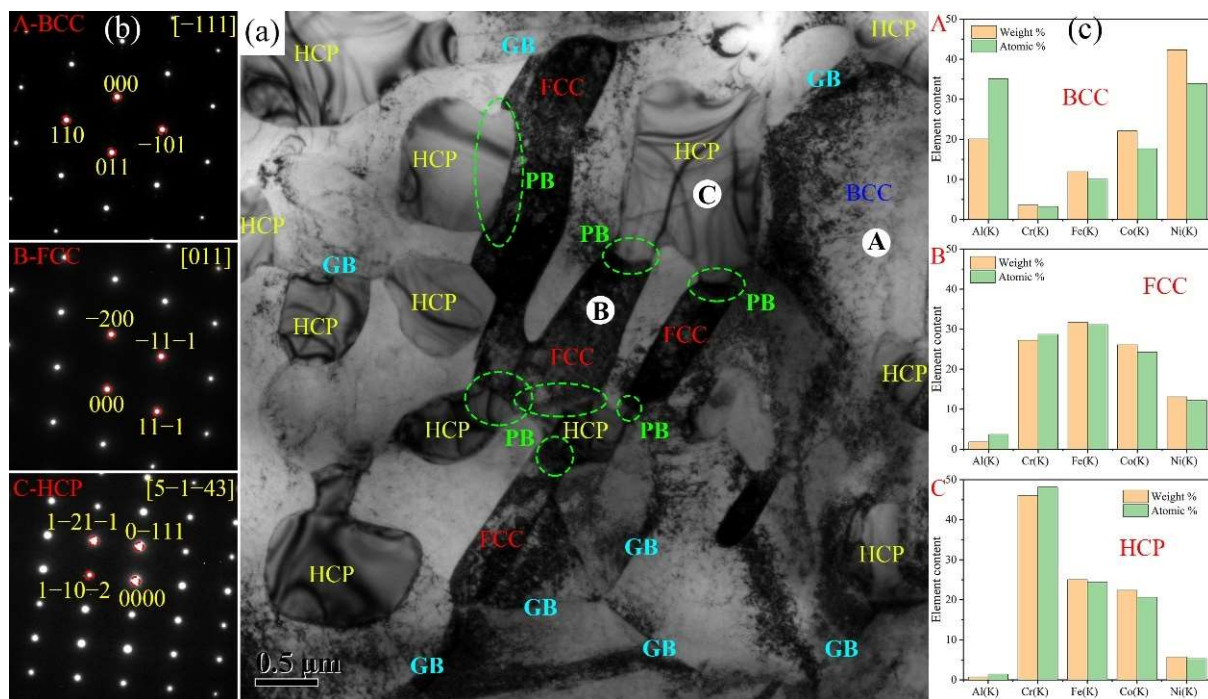


Figure 4. TEM analysis results of the AlCoCrFeNi components after 800 °C high-temperature treatment: (a) high-magnification electron images; (b) selected area diffraction patterns; (c) distribution of alloying elements.

The BCC→FCC transformation in the AlCoCrFeNi component is controlled by the nucleation-growth mechanism [26]. Since the BCC structure has a lower atomic bulk density (68.00%) than the FCC structure (74.00%), it can accommodate small solute atoms (such as Al) more easily [27]. However, when the content of Al element with large atomic radius in the BCC is too much, the lattice distortion would gradually increase and the lattice structure would become unstable. The precipitation of the FCC phase would occur under the combined action of high temperature and high distortion energy. As a result, the BCC to FCC transition occurred in the AlCoCrFeNi component heat-treated at 800 °C, as the temperature is higher than that of the first phase-transition point (Figure 1d).

With increasing heat-treatment temperature, the Al, Ni and Cr elements in the AlCoCrFeNi component began to come together. The Cr element would separate from the Al and Ni to form a Cr-rich phase (i.e., σ phase) when the heat-treatment temperature exceeded the first phase transition temperature (i.e., 639.74 °C) [6–8,11,22]. The σ phase would disappear above 975 °C [21]. Therefore, after the heat treatment at 1000 °C, the AlCoCrFeNi component would contain only FCC and BCC phase structures.

3.2. Mechanical Properties of the AlCoCrFeNi Components

Figure 5 and Table 2 show the compression test results of the AlCoCrFeNi components before and after the high-temperature treatments. Compared with the as-fabricated AlCoCrFeNi component, the strength and plasticity of the component heat-treated at 600 °C did not change significantly. The heat treatment at 800 °C significantly improved the strength and plasticity of the component. The strength of the component heat-treated at 1000 °C remained basically unchanged compared to that of the component heat-treated at 800 °C, but its plasticity improved significantly. Both 800 and 1000 degrees are composed of the FCC phase and BCC phase (Figure 3), so the fracture morphology is similar. Although the compression test results for the four components (as-fabricated and heat-treated) varied, they all failed via brittle fracture, the fracture surfaces exhibited typical cleavage fracture morphologies, as shown in Figure 5(a2–d2).

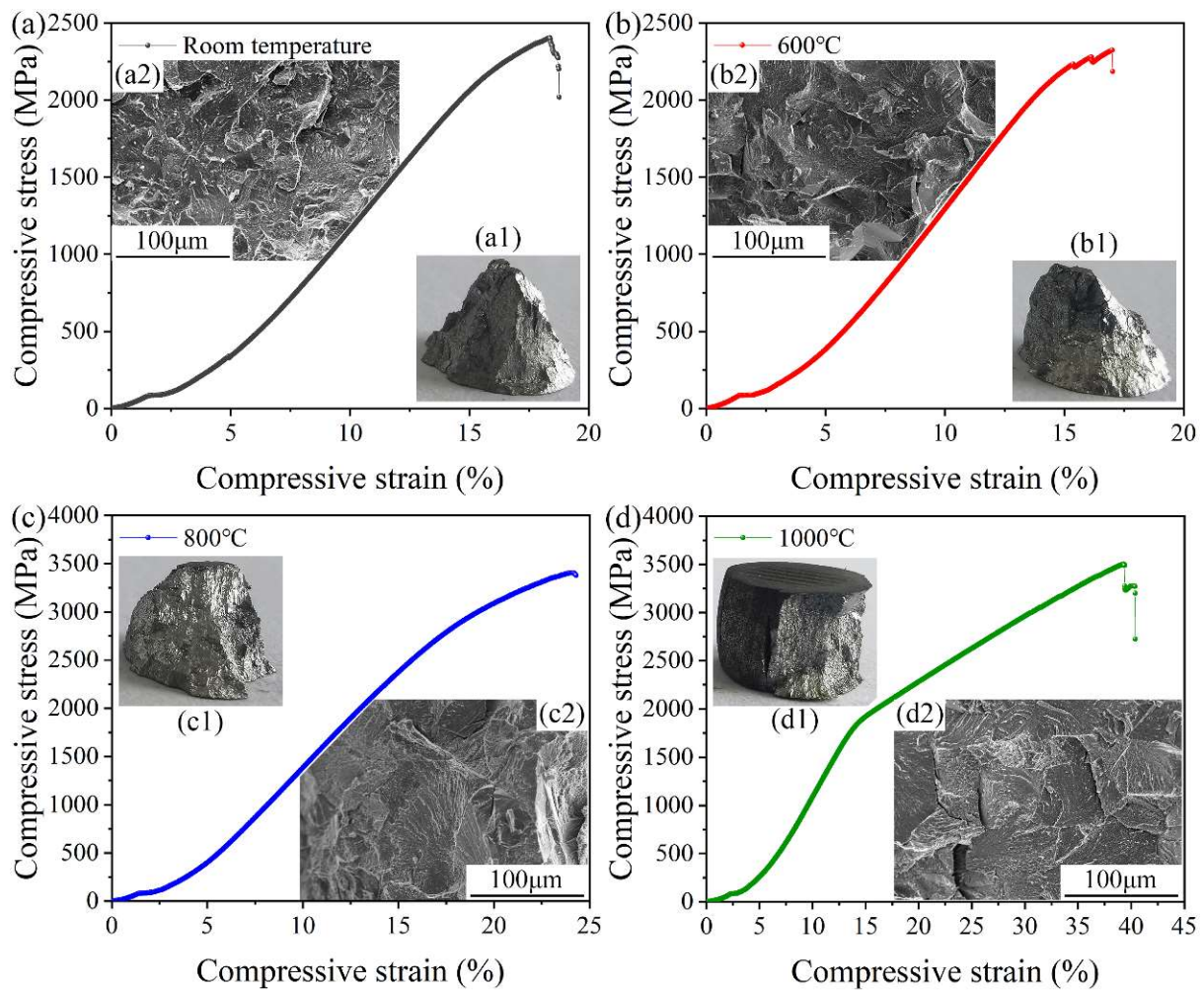


Figure 5. Compression test results, fracture macro morphology and fracture micro morphology of the AlCoCrFeNi components before and after high-temperature treatment: (a, a1 and a2) as-fabricated; heat-treated at (b, b1 and b2) 600 °C; (c, c1 and c2) 800 °C; and (d, d1 and d2) 1000 °C.

Table 2. Compression test results of the AlCoCrFeNi components before and after the high-temperature treatments.

	Compressive Ultimate Strength (MPa)	Strain (%)
As LMD condition	2405.15	18.32
After 5 h at 600 °C	2313.34	17.99
After 5 h at 800 °C	3402.62	24.19
After 5 h at 1000 °C	3502.29	39.36

Figure 6 shows the micro-hardness distributions in the cross-section of the AlCoCrFeNi components before and after high-temperature treatment. The horizontal axis represents the 10 positions selected for hardness testing. The component heat-treated at 800 °C shows the maximum average hardness value and also the largest fluctuation of the hardness values. The as-fabricated component shows the second highest average hardness value. The average hardness of the component heat-treated at 600 °C is slightly lower than that of the as-fabricated one. Both the as-fabricated and 600 °C heat-treated components show small fluctuations of the hardness values. The 1000 °C heat-treated component has the minimum average hardness and also small fluctuation of the hardness value. The high fluctuation of the hardness value of the 800 °C heat-treated component indicates that the hardness

distribution is not uniform, which is not helpful in improving the overall performance of the structural component. This is caused by the incomplete phase transformation of AlCoCrFeNi after heat treatment at 800 °C [9].

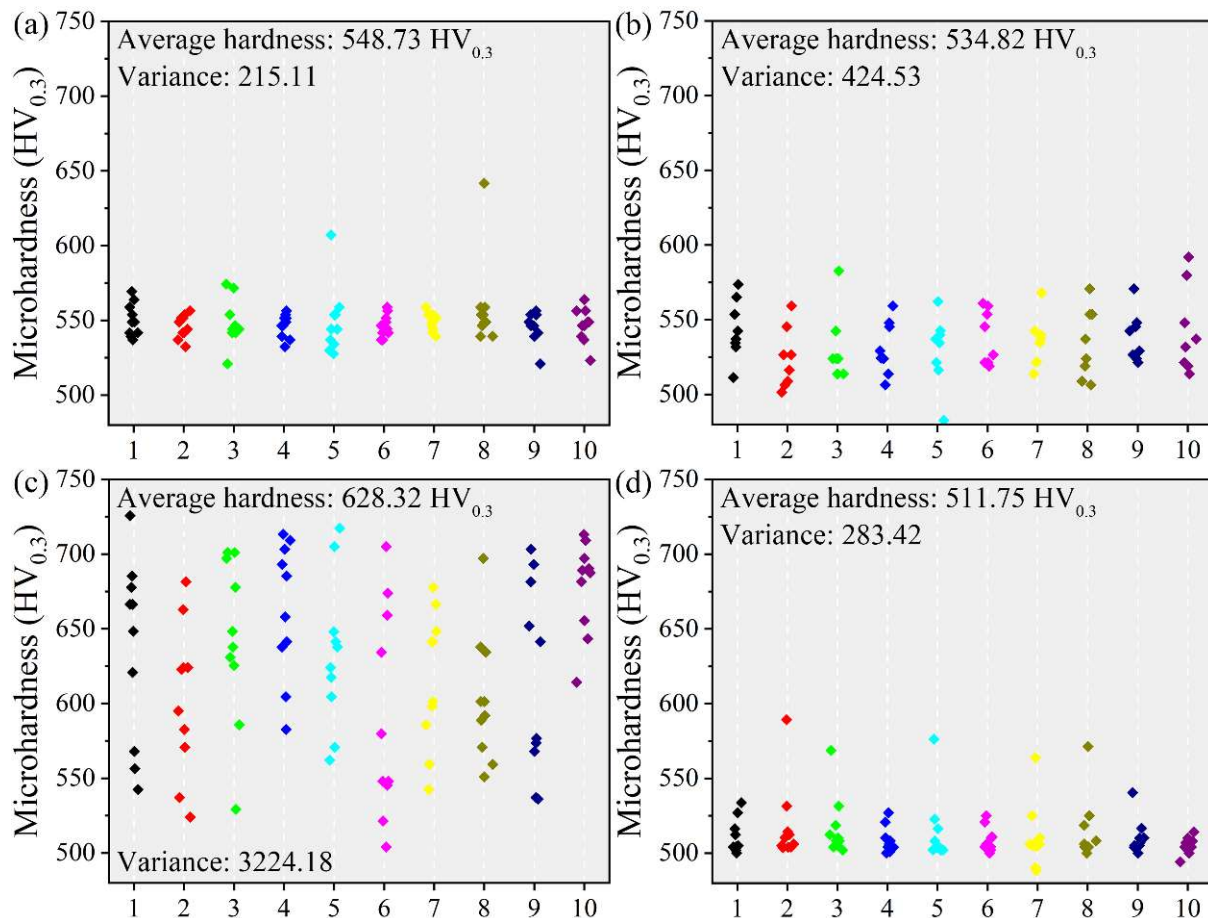


Figure 6. Micro-hardness results of the AlCoCrFeNi components before and after high-temperature treatment: (a) as-fabricated; heat-treated at (b) 600 °C; (c) 800 °C; and (d) 1000 °C.

3.3. Strengthening Mechanism in the AlCoCrFeNi Components

In order to systematically explain the mechanical properties of the AlCoCrFeNi components before and after the high-temperature treatments, the type and evolution of strengthening mechanisms in the components are analyzed based on three factors: fine grain strengthening, dislocation strengthening and precipitation strengthening.

Grain refinement is helpful in improving the yield strength of materials [28,29]. The Grain size was calculated using the statistical method of grain radius of EBSD, as shown in Figure 7. The number on the horizontal axis represents the number of grains. Grain size of the as-fabricated, 600 °C, 800 °C and 1000 °C heat-treated AlCoCrFeNi components was 18.39 μm , 19.81 μm , 19.24 μm and 14.49 μm , respectively. The particle size distribution in Figure 7d has two peaks, around 20 and 4 micrometres. The peak value is about 4 microns, which is caused by the precipitation of the FCC phase. This is why the average grain size is small compared to cases in Figure 7a–c. Grain boundaries are strong obstacles to dislocation movement, and the reduction of the length scale of the characteristic tissue leads to the reduction of the mean free path of dislocation, and thus increases the strength [30,31]. Low-temperature heat treatment has little effect on the grain size of the AlCoCrFeNi component (Figure 7a,b). Therefore, it would also have little effect on the mechanical properties. The grain size of the 800 °C heat-treated component is not much different from that of the as-fabricated and 600 °C heat-treated components. Since the effect of fine-grain strengthening is small, the obvious improvement in strength is due to other strengthening methods. The

reduction of grain size in the 1000 °C heat-treated component could effectively contribute to the improvement of the final strength and plasticity.

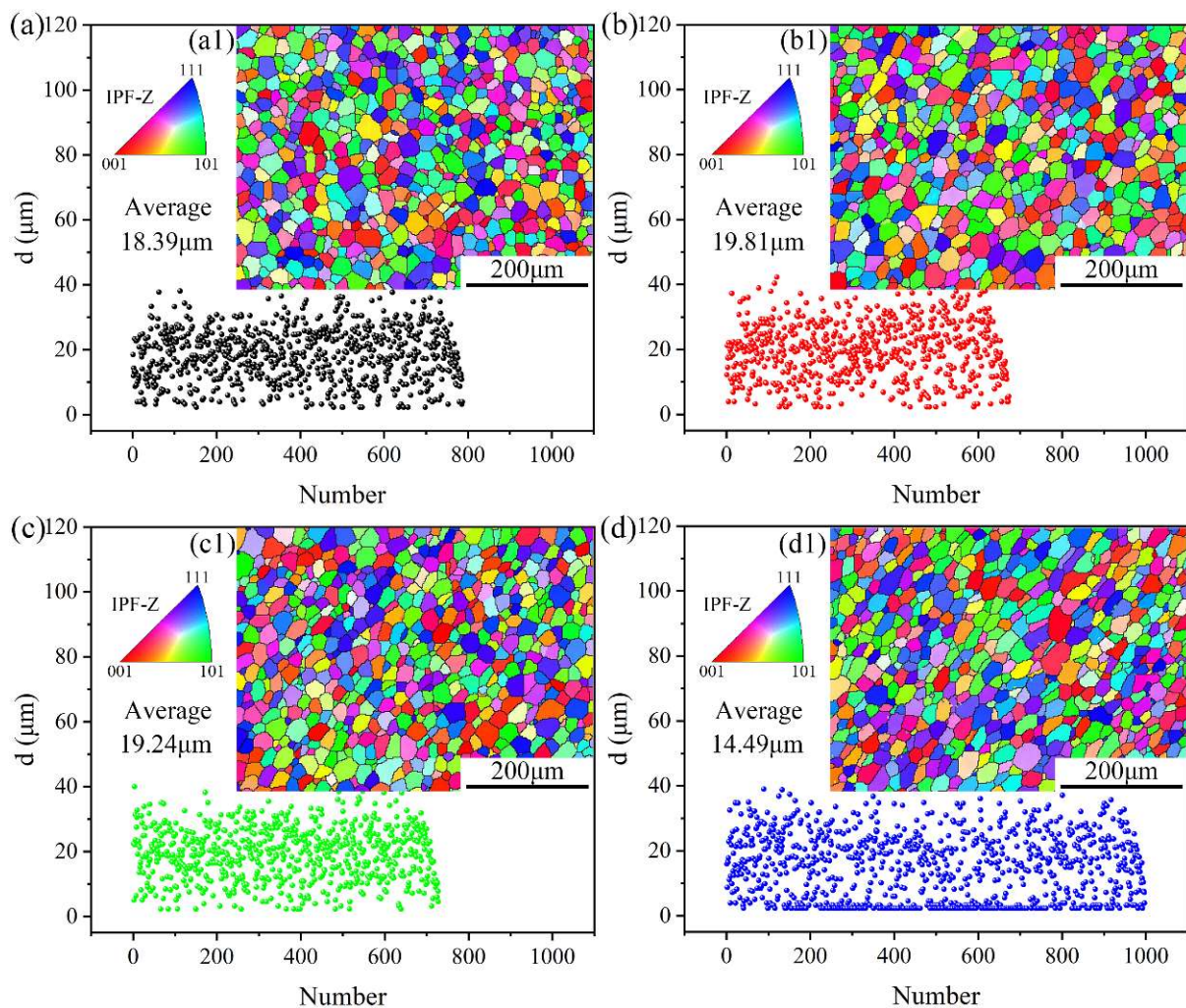


Figure 7. Grain size and IPF detection results of the AlCoCrFeNi components before and after high-temperature treatment: (a,a1) as-fabricated; heat-treated at (b,b1) 600 °C; (c,c1) 800 °C; and (d,d1) 1000 °C.

Generally, in crystalline materials, plastic deformation is caused by dislocation movement. However, as the number of dislocations increases, the interaction between them can hinder their movement to a certain extent [32–34]. In other words, the higher the number of dislocations in the matrix, the higher the strength. The Kernel average misorientation (KAM) method was used to determine the local dislocations from the EBSD data [35]. The KAM's weighted average could be used to quantitatively calculate the geometrically necessary dislocation (GND) density (ρ^{GND}), as expressed in Equation (1) [36,37]:

$$\rho^{\text{GND}} = \frac{2 \text{KAM}_{\text{ave}}}{\mu b} \quad (1)$$

where b is the Burgers vector (2.35×10^{-10}) and μ is the step size. The step size of the AlCoCrFeNi component before/after heat treatment was 0.4 μm .

Figure 8a–d show the distribution of the KAM values. Figure 8(a1–d1) show the KAM diagrams for the as-fabricated and heat-treated AlCoCrFeNi components. Their ρ^{GND} values were $9.728 \times 10^{12} \text{ m}^{-2}$, $7.537 \times 10^{12} \text{ m}^{-2}$, $7.417 \times 10^{12} \text{ m}^{-2}$ ($7.241 \times 10^{12} \text{ m}^{-2}$ for BCC, $1.805 \times 10^{13} \text{ m}^{-2}$ for FCC), and $1.329 \times 10^{13} \text{ m}^{-2}$ ($1.169 \times 10^{13} \text{ m}^{-2}$ for BCC,

$2.424 \times 10^{13} \text{ m}^{-2}$ for FCC), respectively. The low-temperature heat treatment ($600 \text{ }^\circ\text{C}$) could result in little reduction of the dislocation density caused by residual stress in the AlCoCrFeNi component. Two phases, FCC and σ phases, precipitated in the $800 \text{ }^\circ\text{C}$ heat treated component. The brittle σ phase has very weak dislocation tolerance (Figure 4), and the soft FCC phase has a strong dislocation tolerance (Figure 4). However, due to the low content of FCC phase, the dislocation density in the component is basically the same as that in the $600 \text{ }^\circ\text{C}$ heat-treated component. The content of FCC phase in the $1000 \text{ }^\circ\text{C}$ heat-treated component increased significantly, and the σ phase disappeared, resulting in the increase of dislocation density. Therefore, in addition to the fine-grain strengthening, dislocation strengthening also contributed greatly to the strengthening mechanism in the $1000 \text{ }^\circ\text{C}$ heat-treated component. However, dislocation strengthening is not the main strengthening mechanism in the $800 \text{ }^\circ\text{C}$ heat-treated component. Its strengthening mechanism needs to be further discussed. In addition, dislocation strengthening is not an effective strengthening mechanism for low-temperature heat-treated components.

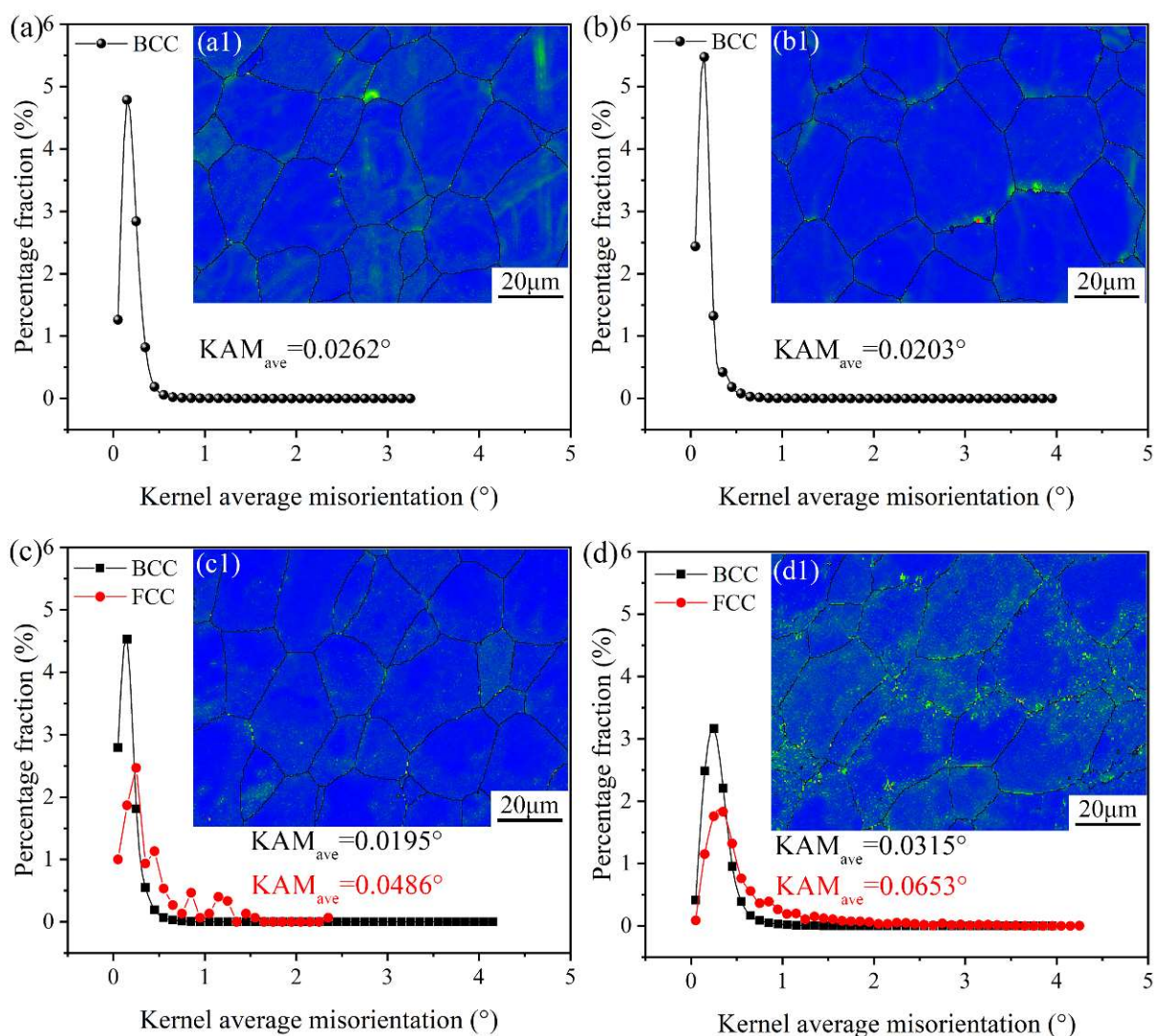


Figure 8. EBSD-KAM detection results and EBSD-KAM distribution curve of the AlCoCrFeNi components before and after high-temperature treatment: (a,a1) as-fabricated; heat-treated at (b,b1) $600 \text{ }^\circ\text{C}$; (c,c1) $800 \text{ }^\circ\text{C}$; and (d,d1) $1000 \text{ }^\circ\text{C}$.

Among the as-fabricated and heat-treated AlCoCrFeNi components, only the $800 \text{ }^\circ\text{C}$ heat treatment promoted the precipitation of the σ phase. Therefore, since fine-grain strengthening and dislocation strengthening mechanisms have been excluded, precipitate

strengthening of brittle, hard phase would be the main strengthening mechanism in the 800 °C heat-treated AlCoCrFeNi component. The σ phase is mainly distributed at the grain boundaries (Figure 4a), resulting in uneven distribution of microhardness and also a significantly increased hardness value, as shown in Figure 6c. During the compression test of the 800 °C heat-treated component, the FCC phase with high dislocation density at the grain boundaries and the pinning effect of the brittle σ phase effectively hindered the dislocation movement and significantly improved the strength. However, the brittle σ phase is prone to crack under the action of forces, reducing the plasticity of the component [38]. Therefore, the strength of the 800 °C heat-treated component is significantly higher than that of the low-temperature heat-treated component, but its plasticity is inferior to that of the 1000 °C heat-treated component.

4. Conclusions

(1) The effects of heat treatment on the phase transition, microstructure and mechanical properties of the AlCoCrFeNi-LMD were systematically studied.

(2) Low temperature heat treatment had no obvious effect on the microstructure and mechanical properties of AlCoCrFeNi component.

(3) Heat treatment (800 °C) beyond the first phase transition temperature (639.74 °C) precipitated FCC and σ phase in the AlCoCrFeNi component, resulting in a 997.47 MPa strength increase and 5.87% plasticity increase. However, the distribution of microhardness values fluctuated greatly.

(4) Heat treatment at 1000 °C made the σ phase disappear in the AlCoCrFeNi component, and the FCC phases distributed near the grain boundaries promoted the further enhance of plasticity, but the hardness value e is reduced to 511.75HV_{0.3}.

Author Contributions: Conceptualization, Y.C. and Z.P.; methodology, J.Y.; software, Z.P.; validation, Y.C.; formal analysis, J.Y.; investigation, J.Y.; resources, J.H.; data curation, J.H.; writing—original draft preparation, Z.P.; writing—review and editing, S.M.M.; visualization, J.Y.; supervision, Z.P.; project administration, Y.C. All authors have read and agreed to the published version of the manuscript.

Funding: This research received no external funding.

Data Availability Statement: Not applicable.

Conflicts of Interest: The authors declare no conflict of interest.

References

1. Yeh, J.W.; Chen, S.K.; Lin, S.J.; Gan, J.Y.; Chin, T.S.; Shun, T.T.; Tsau, C.H.; Chang, S.Y. Nanostructured High-Entropy Alloys with Multiple Principal Elements: Novel Alloy Design Concepts and Outcomes. *Adv. Eng. Mater.* **2004**, *6*, 299–303. [[CrossRef](#)]
2. Wang, F.J.; Zhang, Y.; Chen, G.L.; Davies, H.A. Cooling Rate and Size Effect on the Microstructure and Mechanical Properties of AlCoCrFeNi High Entropy Alloy. *J. Eng. Mater. Technol.* **2009**, *131*, 034501. [[CrossRef](#)]
3. Chou, H.P.; Chang, Y.S.; Chen, S.K.; Yeh, J.W. Microstructure, Thermophysical and Electrical Properties in Al_xCoCrFeNi (0 ≤ x ≤ 2) High-Entropy Alloys. *Mater. Sci. Eng. B* **2009**, *163*, 184–189. [[CrossRef](#)]
4. Shim, S.H.; Pouraliakbar, H.; Hong, S.L. Hierarchical structured as-cast CrFeNiMn_{0.5}Cu_{0.5} high entropy alloy with excellent tensile strength/ductility properties. *Scr. Mater.* **2022**, *210*, 114473. [[CrossRef](#)]
5. Pouraliakbar, H.; Shim, S.H.; Yong, K.K.; Rizzi, M.S.; Sun, I.H. Microstructure evolution and mechanical properties of (CoCrNi)(AlTiZr)(CuFeMo) multicomponent alloy: A pathway through multicomponent alloys toward new superalloys9055. *J. Alloys Compd.* **2021**, *860*, 158412. [[CrossRef](#)]
6. Munitz, A.; Salhov, S.; Hayun, S.; Munitz, A. Heat treatment impacts the micro-structure and mechanical properties of AlCoCrFeNi high entropy alloy. *J. Alloys Compd.* **2016**, *683*, 221–230. [[CrossRef](#)]
7. Liang, J.T.; Cheng, K.C.; Chen, S.H. Effect of heat treatment on the phase evolution and mechanical properties of atomized AlCoCrFeNi high-entropy alloy powders. *J. Alloys Compd.* **2019**, *803*, 484–490. [[CrossRef](#)]
8. Zhou, P.F.; Xiao, D.H.; Yuan, T.C. Microstructure, Mechanical and Corrosion Properties of AlCoCrFeNi High-Entropy Alloy Prepared by Spark Plasma Sintering. *Acta Met. Sin.* **2020**, *33*, 937–946. [[CrossRef](#)]
9. Lin, D.Y.; Zhang, N.N.; He, B.; Jin, B.Q.; Zhang, Y.; Li, D.Y.; Dong, F.Y. Influence of laser re-melting and vacuum heat treatment on plasma-sprayed FeCoCrNiAl alloy coatings. *J. Iron Steel Res. Int.* **2017**, *24*, 1199–1205. [[CrossRef](#)]
10. Wang, L.; Zhang, F.; Yan, S.; Yu, G.; Yin, F. Microstructure evolution and mechanical properties of atmosphere plasma sprayed AlCoCrFeNi high-entropy alloy coatings under post-annealing. *J. Alloys Compd.* **2021**, *872*, 159607. [[CrossRef](#)]

11. Guo, W.M.; Ding, N.; Liu, G.Q.; Jing, C.N.; Xu, H.X.; Liu, L.; Xu, N.; Wu, X.F.; He, J.Q.; Zairi, F. Microstructure evolution of a multi-track AlCoCrFeNi high entropy alloy coating fabricated by laser cladding. *Mater. Charact.* **2022**, *184*, 111660. [[CrossRef](#)]
12. Jang, M.J.; Praveen, S.; Sung, H.J.; Bae, J.W.; Moon, J.; Kim, H.S. High-temperature tensile deformation behavior of hot rolled CrMnFeCoNi high-entropy alloy. *J. Alloys Compd.* **2018**, *730*, 242–248. [[CrossRef](#)]
13. Kim, M.J.; Kang, G.C.; Hong, S.H.; Park, H.J.; Sang, C.M.; Song, G.; Kim, K.B. Understanding microstructure and mechanical properties of $(AlTa_{0.76})_xCoCrFeNi_{2.1}$ eutectic high entropy alloys via thermo-physical parameters. *J. Mater. Sci. Technol.* **2020**, *57*, 131–137. [[CrossRef](#)]
14. Asghari-Rad, P.; Sathiyamoorthi, P.; Bae, J.W.; Moon, J.; Park, J.M.; Zargaran, A.; Kim, H.S. Effect of grain size on the tensile behavior of $V_{10}Cr_{15}Mn_5Fe_{35}Co_{10}Ni_{25}$ high entropy alloy. *Mater. Sci. Eng. A* **2019**, *744*, 610–617. [[CrossRef](#)]
15. Li, Z.M.; Tasan, C.C.; Springer, H.; Gault, B.; Raabe, D. Interstitial atoms enable joint twinning and transformation induced plasticity in strong and ductile high-entropy alloys. *Sci. Rep.* **2017**, *7*, 40704. [[CrossRef](#)]
16. Asabre, A.; Wilms, M.B.; Kostka, A. Laser metal deposition of $Al_{0.6}CoCrFeNi$ with Ti & C additions using elemental powder blends. *Surf. Coat. Technol.* **2021**, *418*, 127233.
17. Park, J.M.; Kim, E.S.; Kwon, H.; Gemagami, P.; Laplanche, G. Effect of heat treatment on microstructural heterogeneity and mechanical properties of 1%C-CoCrFeMnNi alloy fabricated by selective laser melting. *Addit. Manuf.* **2021**, *47*, 102283. [[CrossRef](#)]
18. Huang, L.F.; Sun, Y.N.; Amar, A.; Wu, C.; Li, J. Microstructure evolution and mechanical properties of $Al_xCoCrFeNi$ high-entropy alloys by laser melting deposition. *Vacuum* **2021**, *183*, 109875. [[CrossRef](#)]
19. Sui, Q.X.; Wang, Z.; Wang, J.; Xu, S.; Zhao, F.; Gong, L.; Liu, B.; Liu, J.; Liu, G. The microstructure and mechanical properties of the additive manufactured AlCoCrFeNi high entropy alloy. *Mater. Sci. Eng. A* **2022**, *833*, 142507. [[CrossRef](#)]
20. Niu, P.D.; Li, R.D.; Yuan, T.C.; Zhu, S.Y.; Chen, C.; Wang, M.B.; Huang, L. Microstructures and properties of an equimolar AlCoCrFeNi high entropy alloy printed by selective laser melting. *Intermetallics* **2019**, *104*, 24–32. [[CrossRef](#)]
21. Wang, R.; Zhang, K.; Davies, C.; Wu, X. Evolution of microstructure, mechanical and corrosion properties of AlCoCrFeNi high-entropy alloy prepared by direct laser fabrication. *J. Alloys Compd.* **2017**, *694*, 971–981. [[CrossRef](#)]
22. Sistla, H.R.; Newkirk, J.W.; Liou, F.F. Effect of Al/Ni ratio, heat treatment on phase transformations and microstructure of $Al_xFeCoCrNi_{2-x}$ ($x = 0.3, 1$) high entropy alloys. *Mater. Des.* **2015**, *81*, 113–121. [[CrossRef](#)]
23. Kao, Y.F.; Chen, T.J.; Chen, S.K.; Yeh, J.W. Microstructure and mechanical property of as-cast, -homogenized, and -deformed $Al_xCoCrFeNi$ ($0 \leq x \leq 2$) high-entropy alloys. *J. Alloys Compd.* **2009**, *488*, 57–64. [[CrossRef](#)]
24. Li, C.; Li, J.C.; Zhao, M.; Jiang, Q. Effect of aluminum contents on microstructure and properties of $Al_xCoCrFeNi$ alloys. *J. Alloys Compd.* **2010**, *504*, S515–S518. [[CrossRef](#)]
25. Wang, W.R.; Wang, W.L.; Wang, S.C.; Tsai, Y.C.; Lai, C.H.; Yeh, J.W. Effects of Al addition on the microstructure and mechanical property of $Al_xCoCrFeNi$ high-entropy alloys. *Intermetallics* **2012**, *26*, 44–51. [[CrossRef](#)]
26. Christian, J.W. *The Theory of Transformations in Metals and Alloys*; Pergamon: Oxford, UK, 2002.
27. He, J.Y.; Liu, W.H.; Wang, H.; Wu, Y.; Liu, X.J.; Nieh, T.G.; Lu, Z.P. Effects of Al addition on structural evolution and tensile properties of the FeCoNiCrMn high-entropy alloy system. *Acta Mater.* **2014**, *62*, 105–113. [[CrossRef](#)]
28. Hall, E.O. The deformation and ageing of mild steel: III discussion of results. *Proc. Phys. Soc. Lond. Sect. B* **1951**, *64*, 747–753. [[CrossRef](#)]
29. Xiang, H.G.; Cai, X.; Rong, Y.H. *Fundamentals of Materials Science*, 3rd ed.; Shanghai Jiaotong University Press: Shanghai, China, 2010.
30. Yang, W.F.; Beyerlein, I.J.; Jin, Q.Q.; Ge, H.L.; Xiong, T.; Yang, L.X.; Pang, J.C.; Zhou, Y.T.; Shao, X.H.; Zhang, B. Strength and ductility of bulk Cu/Nb nanolaminates exposed to extremely high temperatures. *Scr. Mater.* **2019**, *166*, 73–77. [[CrossRef](#)]
31. Zheng, S.J.; Zhang, R.F.; Huang, R.; Taniguchi, T.; Ma, X.; Ikuhara, Y.; Beyerlein, I.J. Structure and energetics of nanotwins in cubic boron nitrides. *Appl. Phys. Lett.* **2016**, *109*, 081901. [[CrossRef](#)]
32. Dowling, N.E. Mechanical Behavior of Materials. *Mater. Today* **2005**, *8*, 83–85.
33. Liu, H.H.; Fu, P.X.; Liu, H.W.; Sun, C.; Li, D. Effect of vanadium micro-alloying on the microstructure evolution and mechanical properties of 718H pre-hardened mold steel. *J. Mater. Sci. Technol.* **2019**, *35*, 2526–2536. [[CrossRef](#)]
34. Ma, K.; Wen, H.; Tao, H.; Topping, T.D.; Schoenung, J.M. Mechanical behavior and strengthening mechanisms in ultrafine grain precipitation-strengthened aluminum alloy. *Acta Mater.* **2014**, *62*, 141–155. [[CrossRef](#)]
35. Kamaya, M.; Joao, Q.D.J.; Li, L.M.; Preuss, M. Local plastic strain measurement by EBSD. *Appl. Mech. Mater.* **2007**, *7–8*, 173–179. [[CrossRef](#)]
36. Yan, Z.; Wang, D.; He, X.; Wang, W.X.; Zhang, H.X.; Dong, P.; Li, C.H.; Li, Y.L.; Zhou, J.; Liu, Z. Deformation behaviors and cyclic strength assessment of AZ31B magnesium alloy based on steady ratcheting effect. *Mater. Sci. Eng. A* **2018**, *723*, 212–220. [[CrossRef](#)]
37. Li, J.; Li, H.; Liang, Y.; Liu, P.; Yang, L. The microstructure and mechanical properties of multi-strand, composite welding-wire welded joints of high nitrogen austenitic stainless steel. *Materials* **2019**, *12*, 2944. [[CrossRef](#)]
38. Pharr, G.M. Measurement of mechanical properties by ultra-low load indentation. *Mater. Sci. Eng. A* **1998**, *253*, 151–159. [[CrossRef](#)]